atmosphere

MDPI

Article

Application of WRF-Chem and HYSPLIT Models for Dust Storm Analysis in Central Iran (Case Study of Isfahan Province, 21–23 May 2016)

Farshad Soleimani Sardoo [1,*], Nasim Hossein Hamzeh [2] and Nir Krakauer [3]

[1] Department of Natural Engineering, Faculty of Natural Resources, University of Jiroft, Kerman 78671-55311, Iran
[2] Air and Climate Technology Company (ACTC), Tehran 15996-16313, Iran; nasim_hh@yahoo.com
[3] Department of Civil Engineering, The City College of New York, New York, NY 10031, USA
* Correspondence: f.soleimani@ujiroft.ac.ir or fsoleimani2016@gmail.com

Abstract: Dust is one of the most important problems of human societies in arid and semi-arid areas. This study analyzed the rising and propagation of the dust storm occurring from 21 to 23 May 2016 in Isfahan province (Central Iran) by using the WRF-Chem and HYSPLIT models. The dust storm was visualized using visible imagery and coarse-mode aerosol optical depth data from satellite sensor data, and dust emission and transport were simulated for Central Iran by using WRF-Chem with the AFWA and GOCART schemes. The results show that the dust concentration in Sistan and Baluchistan province and the Persian Gulf was as high as 2000 $\mu g/m^3$, and both schemes estimate the highest amount of dust emissions from the central parts of Iran and the eastern part of Isfahan province. PM10 data of Yazd station was used to verify the model outputs, which showed that the AFWA dust scheme has a higher correlation coefficient with observations (0.62) than the GOCART dust scheme. This case study suggests that WRF-Chem dust schemes simulate dust rising and propagation in Central Iran with reasonably good reliability, though further determination and enhancement are still required for an accurate prediction of dust concentration and extents.

Keywords: dust storm; WRF-chem model; HYSPLYT model; MODIS; GOCART dust scheme; AFWA dust scheme; Isfahan province

Received: 21 January 2025
Revised: 18 March 2025
Accepted: 20 March 2025
Published: 27 March 2025

Citation: Soleimani Sardoo, F.; Hossein Hamzeh, N.; Krakauer, N. Application of WRF-Chem and HYSPLIT Models for Dust Storm Analysis in Central Iran (Case Study of Isfahan Province, 21–23 May 2016). *Atmosphere* **2025**, *16*, 383. https://doi.org/10.3390/atmos16040383

1. Introduction

Dust storms are important natural disasters that affect many people's lives around the world [1–5]. The intensity and frequency of dust storms in arid and semi-arid regions are higher than elsewhere because of the climate and edaphic conditions. Dust storms often occur in desert and plains areas in North America, North Africa, the Gobi Desert, the Middle East, northeastern China, and other regions [6–9]. Such factors as strong wind speed [10–13], a lack of vegetation cover [14–17], a lack of soil moisture, and changing land use [18–21] can be mentioned as the most important and influential ones for the occurrence of dust storms. Dust is emitted as the result of wind erosion that occurs mostly in arid and semi-arid regions. Wind erosion is considered one of the key processes of desertification in arid and semi-arid regions [22–26]. Wind erosion includes the separation, transport, and deposition of mainly soil particles by erosive winds [27,28]. Similarly to dust storms themselves, dry soil, a lack of vegetation, and strong winds are among the most important reasons for wind erosion, which makes dust emission more likely in arid

areas [29]. In recent years, dust events have taken place in the West Asia region with higher frequency and intensity [14,30]. About 30 or up to 50% of all particles entering the atmosphere are dust particles [31]. Numerical models have the ability to calculate the concentration of particles moving downstream by using the emission rates of particles, characteristics of the emission sources, local topography, the meteorology of the research area, and the concentration of environmental particles [31–36]. As a country of the Middle East, Iran is located in the global dust belt. Each year, much damage due to wind erosion is observed in different parts of Iran [18,37–40]. The occurrence of severe dust storms causes severe problems in different sectors related to air quality and human health [41–43], air and road transportation [43], agriculture [44–46], and photovoltaic panel performance [47,48] across Iran. Iran is affected by dust storms mainly originating from external desert dust sources [14,49–51] and, to a lesser extent, from internal deserts [52–54]. In the past two decades, dried lake beds have turned into the largest dust sources [55–58] due to the effects of meteorological drought and anthropogenic water withdrawals. The dried beds of lakes such as Urmia Lake [59–61], Bakhtegan Lake [62,63], and Jazmorian Lake [64,65] contribute to dust storms. Five main dust sources in Iran can be mentioned [6]: Khuzestan Plain in the southwest; the border with Kuwait and Iraq [14,66,67]; the northern coastal plain of the Persian Gulf [68–70]; and two regions in the west of Iran, Tabas in the east [6] and Sistan basin in the southeast [71–73]. Among these five dust sources, the first three also include external dust sources from adjoining countries, but the last two are mostly internal sources [6,14]. Recent studies have highlighted numerical dust prediction models that are being developed to better understand the effects of dust particles on atmospheric dynamics and vice versa. Although the simulation results of numerical models are acceptable, uncertainty remains in the parameters for the rates of dust emission [74], especially in terms of small aerosol particles. The models are used to improve the simulation of dust storms and air quality analysis and forecasting. Until recently, chemical processes in air quality modeling systems were usually simulated separately from meteorological models, with one example being the HYSPLIT model, where independently computed wind fields are then used to simulate particles' forward or back trajectories, but WRF-Chem is an example of a model where all chemical particle transports are calculated while taking into account the feedback on atmospheric dynamics, revealing a more realistic interaction between atmospheric dynamics and dust transport. In version 3.9.1 of the WRF model [39], chemical compound emission, reactions, and transport can be fully analyzed and predicted [75]. The WRF-Chem model includes a dynamic core that is available in two alternative forms, either with Eulerian mass coordinates or the non-hydrostatic NMM mesoscale model (https://www2.acom.ucar.edu/wrf-chem (accessed on 22 July 2024)) [74]. The chemistry part of the model includes calculations related to chemical mechanisms, the optical decomposition of airborne particles, the emission processes of airborne particles from the surface to the atmosphere, processes related to particle removal, and the parameterization of microphysical, dynamic, and thermodynamic processes of airborne particles [74]. Many studies have been conducted regarding the use of the WRF-Chem model to simulate and numerically analyze dust storms with various goals and in different regions, of which [17,76–83] can be mentioned. The purpose of our study is to simulate and numerically analyze the dust storm of 21–23 May 2016 in Central Iran using the WRF-Chem model with the GOCART and AFWA dust schemes. Although the AFWA dust scheme showed better performance in other studies in the west [34] and northwest of Iran in Urmia Lake's dried lake bed [57], its performance in simulating dust rising and propagation in Central Iran has not been investigated. Also, the AOD index is an important parameter in evaluating airborne particles and tracking the temporal and spatial patterns of dust emission. For example, Wang et al. [84] investigated the spatio-temporal characteristics

of dust content in Central Asia and found increasing dust trends in Kazakhstan, Uzbekistan, and Turkmenistan. Also, Dadashi Roudbari and Ahmadi [85], in a study of the southern parts of Iran, identified this area as the center of aerosols in Southwest Asia, which has seen an increase in AOD values in recent years. Sharma et al. [86] also investigated the effect of land use cover (LULC) on AOD in India and found that LULC characteristics were a major determinant of atmospheric aerosol concentrations.

This study investigates a severe dust storm arising from internal minor dust sources in Central Iran that were less investigated in previous studies. This study was conducted in Isfahan province using the WRF-Chem model, and its results were verified with the air pollution monitoring station of Yazd province. In this research, the GOCART and AFWA schemes were used to simulate the dust storm occurring from 21 to 23 May 2016, and the results were compared with the observations.

2. Materials and Methods

2.1. Study Area

Isfahan province, with an area of 107,018 square kilometers, is located between 30 degrees, 43 min to 34 degrees, 37 min north and 49 degrees, 38 min to 55 degrees, 32 min east (Figure 1). The climate of Isfahan province is generally mild and dry. Due to the influence of winds and proximity to the mountainous region in the west and the desert plain in the east and southeast, its climate zones can be divided into desert climate, semi-desert climate, and cold semi-humid climate. According to the report of the synoptic station of Isfahan city, the maximum temperature is 40.6 degrees Celsius, the minimum temperature is −10.6 degrees Celsius, and average annual rainfall is 116.9 mm. The winds that blow in Isfahan province are generally from the west and southwest. Strong winds blow only in the desert areas of the province.

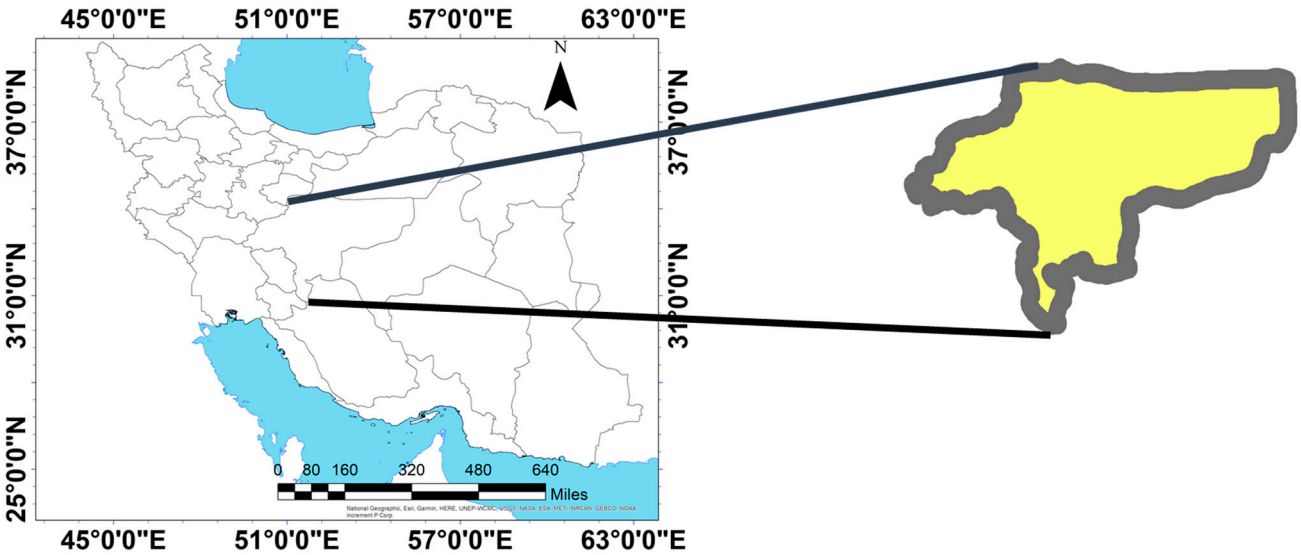

Figure 1. The geographical location of the study area.

In this investigation, based on station observations, the dust storm occurring from 21 to 23 May 2016 was selected as a case study. First, using MODIS satellite images, the extent of the event was verified in Central Iran. Using the HYSPLIT model, the trajectories of dust in the center of Iran were determined, and then the simulation and numerical analysis of the chosen event were performed using the WRF-Chem model, comparing the AFWA and GOCART wind emission schemes and verifying the simulation with station observations. Figure 2 shows a schematic of the strategy implemented in this study.

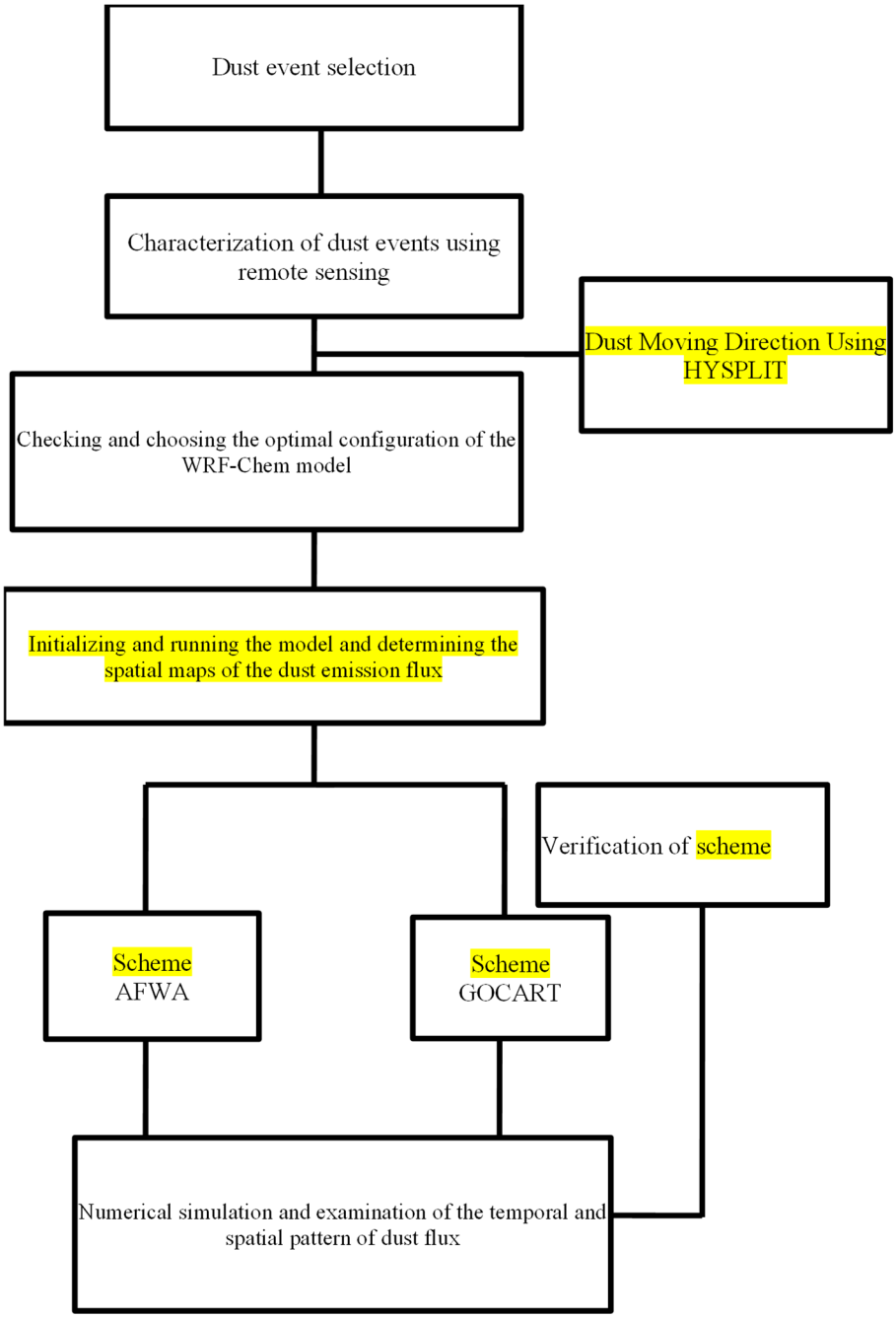

Figure 2. Schematic implementation process of this research.

2.2. Dust Storm Routing Using HYSPLIT Model

HYSPLIT model was used to simulate dust trajectory and identify the origins and areas affected by dust deposition. In order to determine the path of dust movement by this model, gridded meteorological data are needed. The minimum data required to analyze the movement path of dust is the zonal and meridional components of the wind, the vertical speed (omega), and the geopotential height field. Several types of data can be used for the input of the model, but in the study area, the only possibility is to use GDAS data. GDAS data are available at a 1° resolution starting from 2006 and at a 0.5° resolution starting from September 2007.

2.3. WRF-Chem Model

The Weather Research and Forecasting model coupled with Chemistry (WRF-Chem) is widely used for investigations and simulations of regional climate, weather conditions, and pollutants in different parts of the world. In this study, WRF-Chem version 3.9.1 was used for the domain between 25° to 40° N and 44° to 63° with a horizontal resolution of 27 km and 30 vertical sigma levels (from 1000 hPa up to 10 hPa). For initial and boundary conditions, the GFS data produced by NCEP with a 0.5-degree horizontal resolution (~55 km) was used. Furthermore, two dust schemes, GOCART and AFWA, were used for the simulation of dust rising and propagation in the study region.

2.4. GOCART Dust Scheme

This scheme considers potential dust sources based on the erodible fraction. The vertical dust flux from the surface is calculated as follows [84]:

$$F_p = C_G S s_p U_{10}^2 (U_{10} - U_t) U_{10} > U_t \quad (1)$$

where C_G is an experimentally determined constant and is equal to $1.9 \frac{\mu g s^2}{m^5}$, U_{10} is the wind speed at a 10 m height above the surface, U_t is the threshold velocity for the particle wind erosion of p size at a velocity lower than that at which emission does not take place, and s_p is the fraction of each category of dust, which is considered equal to 0.1 for the smallest particle size and 0.25 for other sizes. S is the erodibility function obtained by the following relation [87]:

$$S = \left(\frac{z_{max} - z_i}{z_{max} - z_{min}} \right)^5 \quad (2)$$

Here, S is the probability of accumulation of sediments at point i of the network with height z_i. z_i is the height of the grid cell, and z_{max} and z_{min} are the maximum and minimum heights of the topography at a distance of 10 degrees from the center of the grid cell. In this scheme, five different sizes for ideal spherical dust particles are considered, with radii ranging from 0.1 to 10 μm. The effective radii of the particle classes are assumed to be 0.73, 1.4, 2.4, 4.5, and 8 μm, and all calculations are performed for each class.

2.5. AFWA Dust Schema

The parameterization method presented by Martikorna and Bergamati [88] for the emission of dust particles was implemented in the form of the AFWA dust module by the United States Air Force Meteorological Center in the WRF-Chem model. In the AFWA scheme, the correction factor is applied to u_t as follows:

$$u_t = u_t(D_p) \frac{f(moisture)}{f(roughness)} \quad (3)$$

$$u_t(D_p) = 0.129 \frac{\left[\frac{\rho_p g D_p}{\rho_a} \right]^{0.5} \left[1 + \frac{0.006}{\rho_a g D_p^{2.5}} \right]^{0.5}}{\left[1.928 \left(a D_p^x + b \right)^{0.092} - 1 \right]^{0.5}} u_t = u_t(D_p) \frac{f(moisture)}{f(roughness)} \quad (4)$$

In the above relation, $f(roughness)$ is the drag partition correction. If $f(roughness)$ is equal to 1, it means the surface is smooth. This amount increases with the increase in rocky surfaces, vegetation, and other roughness factors. Currently, the value of $f(roughness)$ is set to 1 for Southwest Asia. This area has a characteristic roughness length of less than 5 m, generally found in deserts and areas with poor vegetation.

In the AFWA scheme, the dust flux caused by the saltation process on the bare soil surface is obtained from the relationship introduced by Kawamura [88] as follows:

$$H(D_p) = C\frac{\rho_a}{g}u^3\left(1+\frac{u_t}{u}\right)\left(1-\frac{u_t^2}{u^2}\right) \quad (5)$$

$$G = \sum H(D_p)dS_{rel}(D_p) \quad (6)$$

The vertical flux of mass dust is calculated based on Martikorna and Bergametti [88], including the correction factor [89]:

$$F_{bulk} = G\alpha \times Erod\alpha = 10^{0.134(\%clay)-6} \quad (7)$$

2.6. WRF Configuration

In order to determine the spatio-temporal propagation of the dust storm in the central areas of Iran, WRF-Chem model version 3.9.1 was used with GFS data for the initial and boundary conditions with a resolution of 0.5 degrees. For the dust scheme in the WRF-Chem model, the AFWA and GOCART dust schemes were used. For this purpose, the model runs with a 27 km resolution with 100 × 102 horizontal grid points and 42 vertical levels. Table 1 shows the detailed physics schemes that the WRF-Chem model used for this study.

Table 1. WRF-Chem model schemes used in this study.

WRF Single-Moment 5-Class Scheme	Microphysics
RRTM Scheme	Long-wave radiation
Goddard Shortwave	Short-wave radiation
Noah Land Surface Model	Surface physics
Yonsei University Scheme	Planetary boundary layer
Grell 3D	Cumulus
AFWA and GOCART Schemes	Dust scheme

3. Results and Discussion

The dust frequencies during the case study period (Figure 3) were taken from the meteorological stations in Iran which were directly affected by the dust storm. Many meteorological stations reported dust in that period across Iran, especially in Western and Central Iran. Most stations recorded under 5 reports in 3 days (yellow circles) or under 10 reports (blue circles). However, some stations reported dust codes of more than 10 and even more than 15 dust reports in 72 h (red and pink circles). The most dust reported was at weather stations in Central Iran, especially Isfahan province. It is worth mentioning that the total number of reported weather codes was 24 reports in 72 h (1 report every 3 h).

The figure shows that the dust storm was widespread and that many Iranian meteorological stations reported the dust storm. Similarly severe and extensive dust storms were investigated in other studies in the Middle East [14,33,90,91].

MODIS imagery confirms that on 21 May 2016, an intense dust storm originated from Dasht-e Lut in SE Iran and occurred in Hamouns in Sistan Basin and covered southeast and Central Iran (Figure 4). Dust plume was observed on 22 and 23 May over Hamoun Lake and Sistan Basin. This dust plume was not so obvious in the MODIS true color image over Central Iran in the following days, but the central weather stations in Iran continued to report dust weather codes in the following days. Weather stations in Isfahan reported intense wind speed on 20 May 2016. For example, Isfahan weather station reported a wind speed of 10 m/s, Ardestan station reported 15 m/s, and Naein station reported 10 m/s on 20th May. This high wind speed promoted dust emission and transport. Figure 4

shows Terra MODIS true color imagery during the examined dust storm in the period of 21–23 May 2016.

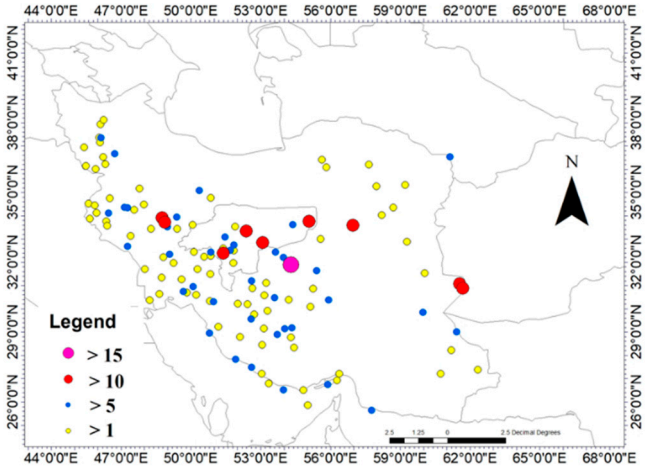

Figure 3. Number of reported dust frequency at all stations in Iran taken from dust-related weather codes in period of 20–22 May 2016. Stations with 1–5 reports in 3 days are shown with yellow circles, and those with 5–10 reports are shown with blue circles. Stations with more than 10 reports in 3 days are shown with red circles, and those with more than 15 dust reports in 72 h are shown with pink circles.

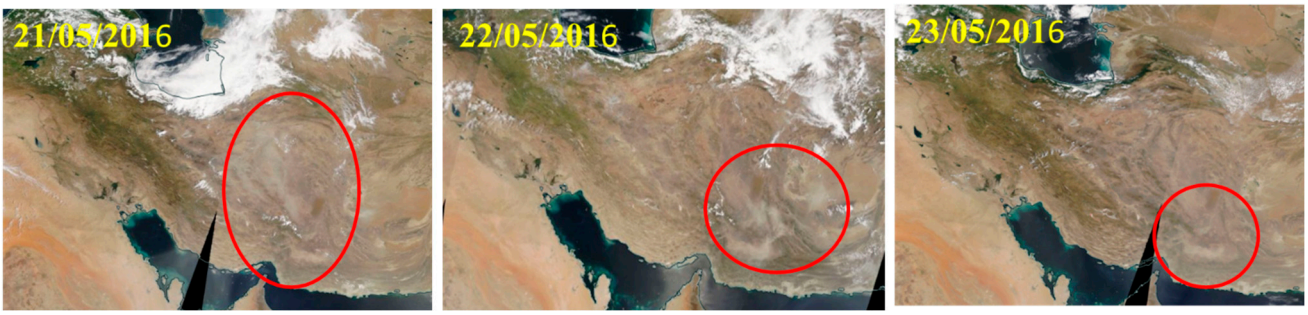

Figure 4. Terra MODIS true color imagery for the dust event in the period of 21–23 May 2016 (Sistan dust storm and Central Iran). The main dust plume is shown by the red circles.

The spatial distributions of Terra-MODIS AOD with a one-degree resolution are shown for the period of 21–23 May 2016 (Figure 5a), and those of TERRA-MODIS AOD 550 nm with a one-degree resolution are shown on 21 May 2016 (Figure 5b). Figure 5a shows the mean aerosol optical depth being more than 0.5 in Eastern, SE, and Central Iran and Isfahan province. In fact, the MODIS 6.1 products show high AOD over more than half of Iran. Since most of the area comprises deserts, such as Loot Desert and Dasht-e Kavīr, and the number of cities is low in this area, the AOD could not be related to other anthropogenic aerosol sources. The number of cities is much higher in Western Iran in comparison with the eastern part, since the eastern part of Iran is mostly covered by deserts relative to the mountain range and plains located in the western part of Iran [53,92–96].

In some parts of the study area, the daily AOD at 550 nm was near 5. Such a high AOD was reported during dust storms in other studies in the Middle East area [91–94] as well. Figure 5b shows the AOD value with a 10 km resolution, which was high in the eastern part of Iran, mostly over 2.5, on 21 May 2016.

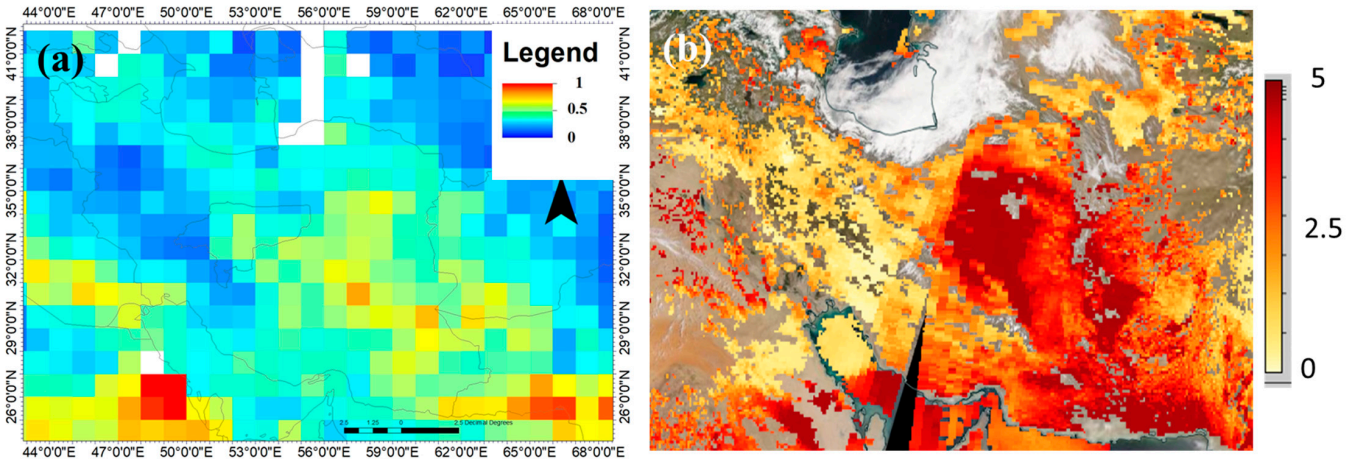

Figure 5. Terra MODIS aerosol optical depth imagery for dust event (**a**) in period of 21–23 May and (**b**) on 21 May 2016.

The spatial distributions of the daily coarse-mode aerosol optical depth (cAOD) of 500 nm over Iran are shown for the period of 21–23 May 2016 (Figure 6a–c). The resolution of the data is 0.5 degrees, and the data are valuable for understanding the impact of dust particles on the atmosphere and climate of any part of the world. The cAOD value shows larger aerosol particles with a radius between 1 and 2.5 µm. The figures show a high cAOD value of 500 nm over Central and southeast Iran in the period of 21–23 May 2023. However, the coarse-mode aerosol optical depth amounts were high on 22 May and decreased drastically on 23 May 2016 in the central area of Iran. These figures are in agreement with TERRA-MODIS AOD 550 nm in Figure 5a that shows a high AOD of 550 nm in the center and southeast of Iran. The figures related to cAOD 500 nm and AOD 550 nm indicate that dust particles increased in the central areas of Iran on 21 May and propagated in the next days.

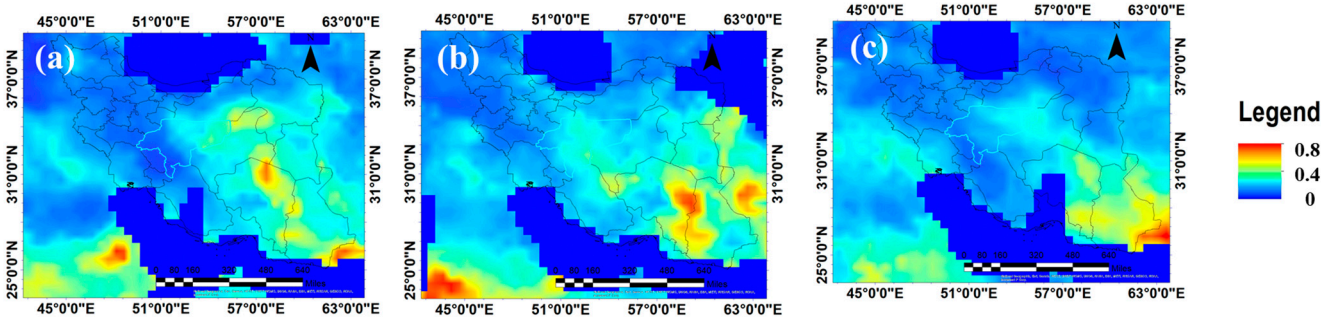

Figure 6. Daily coarse-mode aerosol optical depth (cAOD) of 500 nm over Iran for (**a**) 21 May, (**b**) 22 May, and (**c**) 23 May 2016.

The identification of the dust storm in MODIS imagery is supported by CALIPSO aerosol sub-type classification during CALIPSO overpasses over SW Iran (yellow line in the MODIS imagery).

An intense dust plume was detected over SW and Central Iran (Figure 7). According to the CALIPSO profiles, this dust storm was severe in the south and central parts of Iran, and tropospheric particles (orange color is shown with the number three (Figure 7b)) increased to higher than 6 km in this area. The atmospheric pollution was mostly dust particles in this area on 21 May 2016. Some particles may be related to industrial $PM_{2.5}$. Isfahan is an industrial megacity that has many factories in and around it. Also, it is famous for

its petrochemical and steel industries. However, true color imagery from Terra-MODIS confirms the vast extent of the dust storm event over Central and southeast Iran (Figure 8).

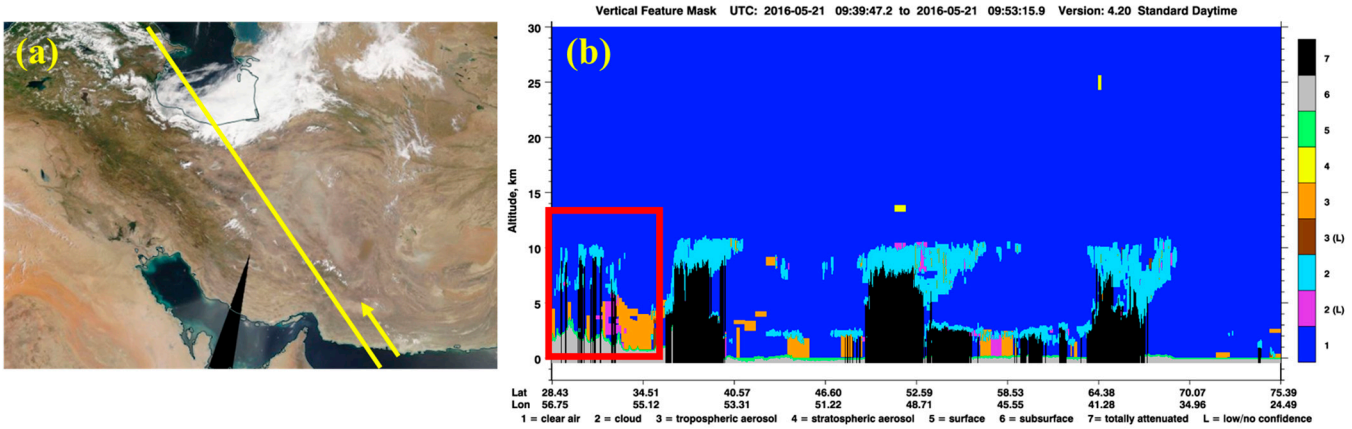

Figure 7. (**a**) True color imagery from the Aqua satellite Moderate-Resolution Imaging Spectroradiometer (MODIS) and Cloud-Aerosol Lidar and Infrared Pathfinder Satellite Observation (CALIPSO) and (**b**) aerosol-type classification on 21 May 2016 over the Middle East. The red box is related to the study area. The CALIPSO orbit path is shown by the yellow line in MODIS imagery, with the yellow arrows showing the direction of the overpass (1. clear air (blue); 2. cloud (purple); 3. tropospheric aerosol (orange); 4. stratospheric aerosol (yellow); 5. surface (green); 6. subsurface (Birch); 7. totally attenuated (black)).

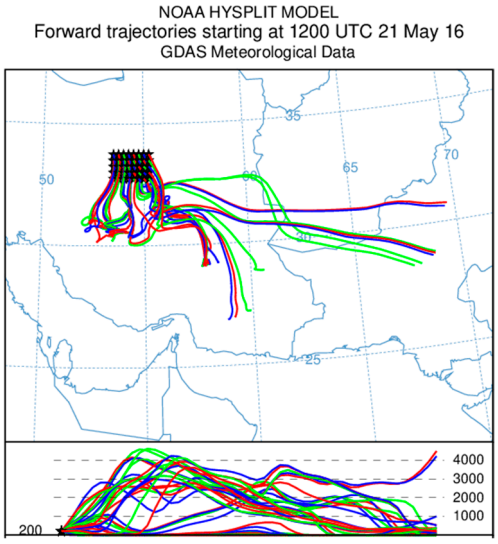

Figure 8. Two-day backward trajectory matrix from HYSPLIT model for air masses at 200 m above ground in affected east part of Isfahan province.

HYSPLIT outputs indicate the prevailing winds from the east and southeast directions (Figure 8). The trajectories show a twist near the study area. It appears that the dust plume originated from Central and SE Iran. Mesbahzadeh and Ahmadi [97] confirmed that the spring's dominant wind direction is westerly in Kashan station, located in Isfahan province in Central Iran. Also, their study showed that the dominant wind direction is westerly and north-westerly in the Yazd plain in Central Iran. But in this case, the dominant wind direction was easterly, bringing dust emissions from source areas to the east and southeast to Central Iran. Figure 8 shows 48 h backward trajectories from the HYSPLIT model for air masses 200 m above the ground in the affected east part of Isfahan province.

The simulations with both WRF-Chem dust schemes revealed a high dust concentration over Sistan basin in the period of 21–22 May 2016 (Figure 9), comparable to levels recorded in this area several times in the past [14,71,96]. The model found present high dust concentrations (higher than 2000 mg/m^{-3}) over the Persian Gulf and SW of it. A high dust concentration over this area was reported in many studies [69,98–102]. Furthermore, simulations with both dust schemes show the severe dust storm in Isfahan province, especially in the east of the province at 00:00 UTC on 21 May 2021. The GOCART dust scheme showed a higher dust concentration over eastern Isfahan province, while the AFWA dust scheme shows a severe dust storm outside of Isfahan province that spreads over a bigger area. The dust storm in Central Iran was therefore simulated with different magnitudes and spatial extents across the two different dust schemes, although using both of them led to simulating a dust storm in the period of 21–22 May 2016 in Isfahan province and Central Iran. As explained above, the surface dust concentration in the GOCART dust scheme depends on the wind velocity in 10 m, while the AFWA dust scheme uses threshold friction velocities for the calculation of the dust surface concentration.

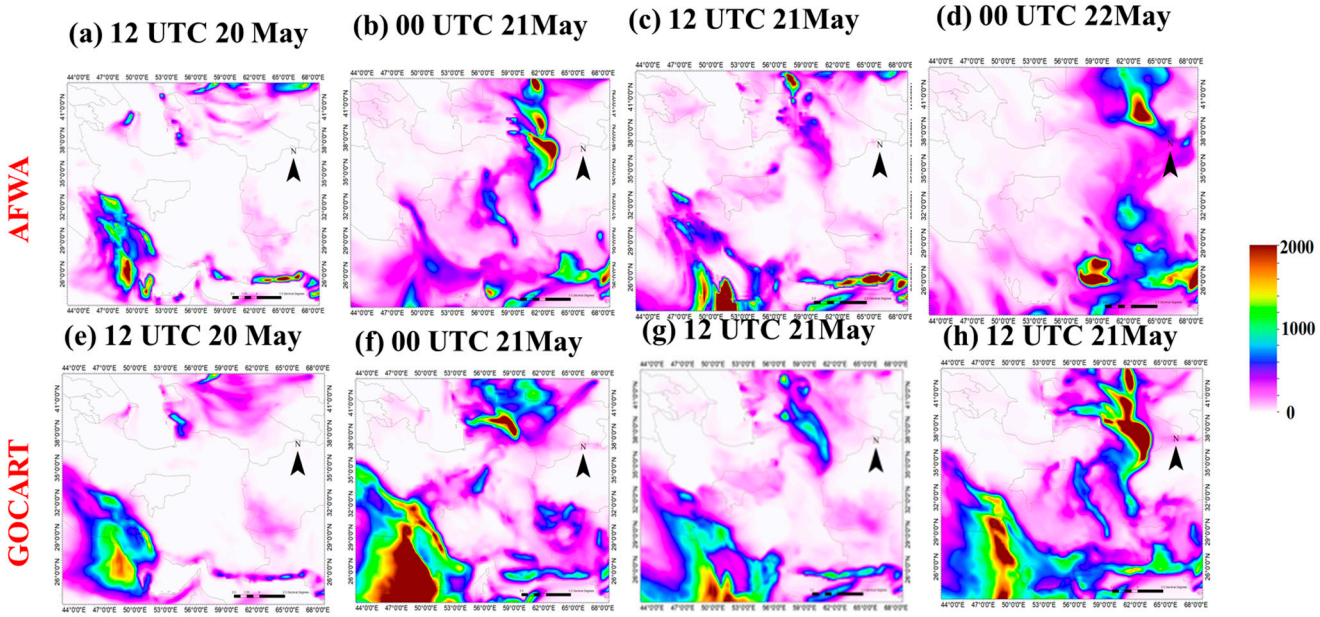

Figure 9. Spatial distribution of surface dust concentration (PM_{10}, μgm^{-3}) according to WRF-Chem models with two dust schemes at 00:00 UTC and 12:00 UTC in period of 20–22 May 2016.

Both dust schemes underestimated PM_{10} amounts observed at Yazd station, with the simulated concentrations being more similar to each other than to the observations (Figure 10). Also, the maximum simulated surface concentration occurred earlier in the storm compared to the measurements. Similarly, Abadi et al. [57] showed that PM_{10} amounts in the AFWA and GOCART dust schemes peaked 12 h sooner than the measured ones in the Urmia Lake dust storm. Zhao et al. [103] showed all five WRF-Chem dust schemes underestimated or overestimated the surface dust concentration in NW China and, in particular, the GOCART dust scheme underestimated dust emission. Tsarpalis et al. [104] showed that the GOCART and AFWA dust schemes underestimated PM_{10} and AOD amounts in Central Asia in a dust storm case study of 12–15 July 2016. Also, Karami et al. [105] showed that the WRF-Chem simulation with the AFWA dust scheme underestimated PM_{10} amounts in Sistan dust cases in SE Iran. The simulation of dust might depend on subscale topography and soil texture, for example, in dry lake beds, that is not being well resolved. Figure 10 shows the temporal evolution of the PM_{10} concentrations

(μgm^{-3}) measured at air monitoring stations in Yazd in Central Iran and simulated by two dust schemes of WRF-Chem in the period of 23–26 May 2016.

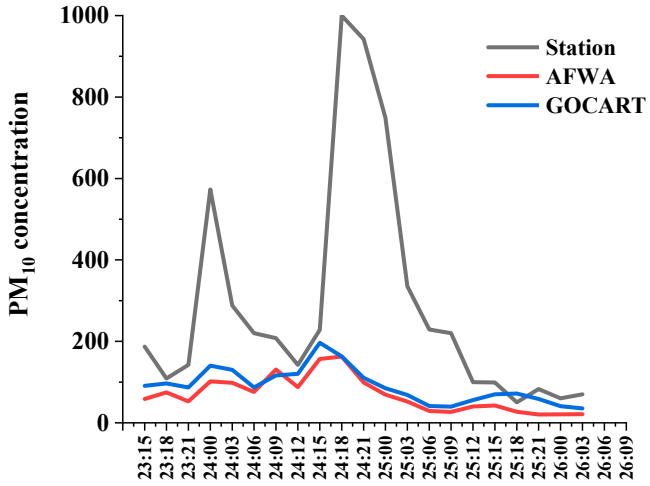

Figure 10. Temporal evolution of PM10 concentrations (μgm^{-3}) measured at air monitoring stations in Yazd and simulated by two dust schemes implemented in WRF-Chem in period of 23–26 May 2016.

The correlation coefficient between the AFWA dust scheme and measured PM_{10} is high (0.62), and it was higher than the GOCART dust scheme (0.52), as shown in Table 2 However, the mean absolute error (MAE) was 299.03 μgm^{-3} in the AFWA dust scheme and it was 209.12 μgm^{-3} in the GOCART dust scheme in Yazd station in the study period. Table 2 shows the correlation and MAE of the output of the two WRF-Chem dust schemes and measured PM_{10} in Yazd station in Central Iran. The results obtained by the station show that the MAE, RMSE, and bias errors related to the GOCART dust scheme were lower than the AFWA dust scheme. Furthermore, the negative mean bias shows both dust schemes underestimated PM_{10} in Yazd station in the center of Iran. The AFWA dust scheme underestimated PM_{10} amounts somewhat more than the GOCART dust scheme.

Table 2. Correlation, MAE of output of two WRF-Chem dust schemes, and measured PM_{10} in Yazd station in Central Iran.

Dust Scheme	AFWA	GOCART
Correlation	0.62	0.52
MAE	299.03	209.12
RMSE	359.2	352.3
Bias	−224.67	−204.25

4. Conclusions

Dust storms are one of the main problems of dry areas. Isfahan province is exposed to these storms by being located near the Lut and central deserts of Iran. Also, the Gav Khooni wetland is considered to be a source of dust in this province in times of water shortage. Zayandeh Rood, as the largest central river of Iran, which flows into the Gav Khooni wetland, has faced water shortage and drought due to various climatic and human reasons, leading it to become a source of dust in Isfahan province. In this study, by using remote sensing data as well as dust-related codes from weather station reports, the event of 21–23 May 2016 was selected as a widespread and severe phenomenon for simulation and numerical analysis. MODIS and CALIPSO satellite images were used to visualize the prevalence and severity of dust, which was confirmed and simulated with the WRF-Chem

model. In this model, AFWA and GOCART schemes were chosen to simulate dust emission. The finding with both dust schemes visualized the severe dust storm in Isfahan province, particularly in the east of the province, at 00:00 UTC 21 May 2021, but the GOCART dust scheme showed a higher dust concentration over the east of Isfahan province, while the results with the AFWA dust scheme showed a concentrated severe dust storm outside of Isfahan province that spread over a bigger area. The dust storm in Central Iran was simulated with different magnitudes and spatial extents between the two dust schemes, but in both cases, there was a dust storm simulated in the period of 21–22 May 2016 in Isfahan province and Central Iran. Finally, in order to validate the results of the schemes, the air monitoring station of Yazd was used, which is located in the neighborhood of Isfahan province. The results show that the correlation coefficient between the AFWA dust scheme and the measured PM10 (0.62) were higher than those of the GOCART dust scheme (0.52). But the MAE was 299.03 μgm^{-3} in the AFWA dust scheme, and it was 209.12 μgm^{-3} in the GOCART dust scheme in Yazd station in the study period, showing that the error between the GOCART dust scheme simulation and the station data was lower than the AFWA dust scheme, although both schemes did not simulate the peak observed dust concentration well. For future studies, we suggest conducting more investigations of the dust sources in desert areas in Central Iran and how their emission rates can be accurately parametrized. Although high dust frequencies in southwest, west, and southeast Iran have led to more attention being paid to air pollution in those areas, central dust sources in Iran have become more active in recent years and also need more attention from scientists and the authorities. One of the most important weaknesses of this study is the lack of validation stations, so it is suggested that the national environmental organization provide data from air pollution monitoring stations to research centers and universities.

Author Contributions: All authors contributed to the study's conception and design. Material preparation, data collection, and analysis were performed by F.S.S. The first draft of the manuscript was written by N.H.H. The final draft of the manuscript was written by N.K. All authors have read and agreed to the published version of the manuscript.

Funding: This research received no external funding.

Institutional Review Board Statement: Not applicable.

Informed Consent Statement: Not applicable.

Data Availability Statement: Data sets supporting reported results are: https://www.ready.noaa.gov/hypub-bin/trajtype.pl?runtype=archive (accessed on 18 March 2025).

Acknowledgments: We are thankful from the University of Jiroft. Also, we are thankful from NOAA for availability HYSPLIT model. We appreciate Department of Environment, Iran for PM_{10} data in Yazd station. The authors apriciate from Nasa for providing CALIPSO satellite image and Giovanni NASA for providing AOD data over the MIDDLE East area.

Conflicts of Interest: Nasim Hossein Hamzeh is an employee of the Air and Climate Technology Company (ACTC). This paper reflects the views of the scientists and not the company. The authors declare no conflicts of interest.

References

1. Miri, A.; Ahmadi, H.; Ekhtesasi, M.R.; Panjehkeh, N.; Ghanbari, A. Environmental and socio-economic impacts of dust storms in Sistan Region, Iran. *Int. J. Environ. Stud.* **2009**, *66*, 343–355.
2. Goudie, A.S. Dust storms and human health. In *Extreme Weather Events and Human Health: International Case Studies*; Springer: Berlin/Heidelberg, Germany, 2020; pp. 13–24.
3. Ghosh, T.; Pal, I. Dust storm and its environmental implications. *J. Eng. Comput. Appl. Sci. (JECAS)* **2014**, *3*, 30–37.

4. Karshieva, D.R.; Nazarova, F.A.; Tolibova, Z.H. Atmospheric dust and its effects on human health. *Acad. Int. Multidiscip. Res. J.* **2021**, *11*, 1168–1172.
5. Xu, L.Y.; Shu, X. Aggregate human health risk assessment from dust of daily life in the urban environment of Beijing. *Risk Anal.* **2014**, *34*, 670–682.
6. Alizadeh-Choobari, O.; Ghafarian, P.; Owlad, E. Temporal variations in the frequency and concentration of dust events over Iran based on surface observations. *Int. J. Climatol.* **2016**, *36*, 2050–2062.
7. Nodej, T.M.; Rezazadeh, M. The spatial distribution of critical wind erosion centers according to the dust event in Hormozgan province (south of Iran). *Catena* **2018**, *167*, 340–352.
8. Abadi, A.R.S.; Hamzeh, N.H.; Chel Gee Ooi, M.; Kong, S.S.K.; Opp, C. Investigation of two severe shamal dust storms and the highest dust frequencies in the south and southwest of Iran. *Atmosphere* **2022**, *13*, 1990. [CrossRef]
9. Gherboudj, I.; Beegum, S.N.; Ghedira, H. Identifying natural dust source regions over the Middle-East and North-Africa: Estimation of dust emission potential. *Earth-Sci. Rev.* **2017**, *165*, 342–355. [CrossRef]
10. Hamzeh, N.H.; Abadi, A.R.S.; Kaskaoutis, D.G.; Mirzaei, E.; Shukurov, K.A.; Sotiropoulou, R.E.P.; Tagaris, E. The importance of wind simulations over dried lake beds for dust emissions in the Middle East. *Atmosphere* **2023**, *15*, 24. [CrossRef]
11. Saadatabadi, A.R.; Hamzeh, N.H.; Kaskaoutis, D.G.; Ghasabi, Z.; Penchah, M.M.; Sotiropoulou, R.E.P.; Habibi, M. Optimization and evaluation of the Weather Research and Forecasting (WRF) model for wind energy resource assessment and mapping in Iran. *Appl. Sci.* **2024**, *14*, 3304. [CrossRef]
12. Csavina, J.; Field, J.; Félix, O.; Corral-Avitia, A.Y.; Sáez, A.E.; Betterton, E.A. Effect of wind speed and relative humidity on atmospheric dust concentrations in semi-arid climates. *Sci. Total Environ.* **2014**, *487*, 82–90. [CrossRef] [PubMed]
13. Grini, A.; Myhre, G.; Zender, C.S.; Isaksen, I.S. Model simulations of dust sources and transport in the global atmosphere: Effects of soil erodibility and wind speed variability. *J. Geophys. Res. Atmos.* **2005**, *110*, 14–28. [CrossRef]
14. Hamzeh, N.H.; Kaskaoutis, D.G.; Rashki, A.; Mohammadpour, K. Long-term variability of dust events in southwestern Iran and its relationship with the drought. *Atmosphere* **2021**, *12*, 1350. [CrossRef]
15. Khusfi, Z.E.; Khosroshahi, M.; Roustaei, F.; Mirakbari, M. Spatial and seasonal variations of sand-dust events and their relation to atmospheric conditions and vegetation cover in semi-arid regions of central Iran. *Geoderma* **2020**, *365*, 114225. [CrossRef]
16. Yan, Y.; Xu, X.; Xin, X.; Yang, G.; Wang, X.; Yan, R.; Chen, B. Effect of vegetation coverage on aeolian dust accumulation in a semiarid steppe of northern China. *Catena* **2011**, *87*, 351–356. [CrossRef]
17. Kim, D.; Chin, M.; Remer, L.A.; Diehl, T.; Bian, H.; Yu, H.; Brown, M.E.; Stockwell, W.R. Role of surface wind and vegetation cover in multi-decadal variations of dust emission in the Sahara and Sahel. *Atmos. Environ.* **2017**, *148*, 282–296. [CrossRef]
18. Nazarpour, A.; Ghanavati, N.; Watts, M.J. Spatial distribution and human health risk assessment of mercury in street dust resulting from various land-use in Ahvaz, Iran. *Environ. Geochem. Health* **2018**, *40*, 693–704. [CrossRef]
19. Ahmadi-Molaverdi, M.; Jabbari, I.; Fathnia, A. Relationship Between Land Use Changes and the Production of Dust Sources in Kermanshah Province, Iran. *Chin. Geogr. Sci.* **2021**, *31*, 1057–1069. [CrossRef]
20. Lee, J.A.; Gill, T.E.; Mulligan, K.R.; Acosta, M.D.; Perez, A.E. Land use/land cover and point sources of the 15 December 2003 dust storm in southwestern North America. *Geomorphology* **2009**, *105*, 18–27. [CrossRef]
21. Wang, X.; Zhou, Z.; Dong, Z. Control of dust emissions by geomorphic conditions, wind environments and land use in northern China: An examination based on dust storm frequency from 1960 to 2003. *Geomorphology* **2006**, *81*, 292–308. [CrossRef]
22. Duniway, M.C.; Pfennigwerth, A.A.; Fick, S.E.; Nauman, T.W.; Belnap, J.; Barger, N.N. Wind erosion and dust from US drylands: A review of causes, consequences, and solutions in a changing world. *Ecosphere* **2019**, *10*, e02650.
23. Webb, N.P.; Strong, C.L. Soil erodibility dynamics and its representation for wind erosion and dust emission models. *Aeolian Res.* **2011**, *3*, 165–179.
24. Shao, Y.; Jung, E.; Leslie, L.M. Numerical prediction of northeast Asian dust storms using an integrated wind erosion modeling system. *J. Geophys. Res. Atmos.* **2002**, *107*, AAC-21.
25. Kaskaoutis, D.G.; Francis, D.; Rashki, A.; Chaboureau, J.P.; Dumka, U.C. Atmospheric dynamics from synoptic to local scale during an intense frontal dust storm over the Sistan Basin in winter 2019. *Geosciences* **2019**, *9*, 453. [CrossRef]
26. Kaskaoutis, D.G.; Rashki, A.; Houssos, E.E.; Mofidi, A.; Goto, D.; Bartzokas, A.; Francois, P.; Legrand, M. Meteorological aspects associated with dust storms in the Sistan region, southeastern Iran. *Clim. Dyn.* **2015**, *45*, 407–424.
27. Lee, J.A.; Gill, T.E. Multiple causes of wind erosion in the Dust Bowl. *Aeolian Res.* **2015**, *19*, 15–36.
28. Hoffmann, C.; Funk, R.; Reiche, M.; Li, Y. Assessment of extreme wind erosion and its impacts in Inner Mongolia, China. *Aeolian Res.* **2011**, *3*, 343–351.
29. Shao, Y.; Dong, C.H. A review on East Asian dust storm climate, modelling and monitoring. *Glob. Planet. Change* **2006**, *52*, 1–22.
30. Azizi, G.; Shamsipour, A.A.; Miri, M.; Safarrad, T. Statistic and synoptic analysis of dust phenomena in west of Iran. *J. Environ. Stud.* **2012**, *38*, 123–134.
31. Alfaro, S.C. Influence of soil texture on the binding energies of fine mineral dust particles potentially released by wind erosion. *Geomorphology* **2008**, *93*, 157–167.

32. Nickovic, S.; Vukovic, A.; Vujadinovic, M.; Djurdjevic, V.; Pejanovic, G. High-resolution mineralogical database of dust-productive soils for atmospheric dust modeling. *Atmos. Chem. Phys.* **2012**, *12*, 845–855. [CrossRef]
33. Karegar, E.; Hossein Hamzeh, N.; Bodagh Jamali, J.; Ranjbar Saadat Abadi, A.; Moeinaddini, M.; Goshtasb, H. Numerical simulation of extreme dust storms in east of Iran by the WRF-Chem model. *Nat. Hazards* **2019**, *99*, 769–796. [CrossRef]
34. Mohammadpour, K.; Hassan, E.M.; Kaskaoutis, D.G.; Rashki, A.; Hamzeh, N.H.; Rahimi, S. Monitoring and simulation of a 7-day dust episode and associated dust radiative forcing over the Middle East via synergy of satellite observations, reanalysis datasets and regional/numerical models. *Atmos. Res.* **2025**, *316*, 107948.
35. Kaskaoutis, D.G.; Prasad, A.K.; Kosmopoulos, P.G.; Sinha, P.R.; Kharol, S.K.; Gupta, P.; El-Askary, H.M.; Kafatos, M. Synergistic use of remote sensing and modeling for tracing dust storms in the Mediterranean. *Adv. Meteorol.* **2012**, *2012*, 861026. [CrossRef]
36. Kang, J.Y.; Yoon, S.C.; Shao, Y.; Kim, S.W. Comparison of vertical dust flux by implementing three dust emission schemes in WRF/Chem. *J. Geophys. Res. Atmos.* **2011**, *116*, D09202. [CrossRef]
37. Akhzari, D.; Farokhzadeh, B.; Saeedi, I.; Goodarzi, M. Effects of wind erosion and soil salinization on dust storm emission in western Iran. *J. Rangel. Sci.* **2015**, *5*, 37–48.
38. Ebrahimi-Khusfi, Z.; Mirakbari, M.; Ebrahimi-Khusfi, M.; Taghizadeh-Mehrjardi, R. Impacts of vegetation anomalies and agricultural drought on wind erosion over Iran from 2000 to 2018. *Appl. Geogr.* **2020**, *125*, 102330. [CrossRef]
39. Karami, S.; Hamzeh, N.H.; Abadi, A.R.S.; Madhavan, B.L. Investigation of a severe frontal dust storm over the Persian Gulf in February 2020 by CAMS model. *Arab. J. Geosci.* **2021**, *14*, 2041. [CrossRef]
40. Miri, A.; Middleton, N. Long-term impacts of dust storms on transport systems in south-eastern Iran. *Nat. Hazards* **2022**, *114*, 291–312. [CrossRef]
41. Goudarzi, G.; Daryanoosh, S.M.; Godini, H.; Hopke, P.K.; Sicard, P.; De Marco, A.; Rad, H.D.; Harbizadeh, A.; Jahedi, F.; Mohammadi, M.J.; et al. Health risk assessment of exposure to the Middle-Eastern Dust storms in the Iranian megacity of Kermanshah. *Public Health* **2017**, *148*, 109–116. [CrossRef]
42. Neisi, A.; Goudarzi, G.; Akbar Babaei, A.; Vosoughi, M.; Hashemzadeh, H.; Naimabadi, A.; Mohammadi, M.J.; Hashemzadeh, B. Study of heavy metal levels in indoor dust and their health risk assessment in children of Ahvaz city, Iran. *Toxin Rev.* **2016**, *35*, 16–23.
43. Behrooz, R.D.; Kaskaoutis, D.G.; Grivas, G.; Mihalopoulos, N. Human health risk assessment for toxic elements in the extreme ambient dust conditions observed in Sistan, Iran. *Chemosphere* **2021**, *262*, 127835.
44. Maleki, T.; Sahraie, M.; Sasani, F.; Shahmoradi, M. Impact of dust storm on agricultural production in Iran. *Int. J. Agric. Sci. Res. Technol. Ext. Educ. Syst. (IJASRT EESs)* **2017**, *7*, 19–26.
45. Boroughani, M.; Mohammadi, M.; Mirchooli, F.; Fiedler, S. Assessment of the impact of dust aerosols on crop and water loss in the Great Salt Desert in Iran. *Comput. Electron. Agric.* **2022**, *192*, 106605.
46. Hamzeh, N.H.; Shukurov, K.; Mohammadpour, K.; Kaskaoutis, D.G.; Saadatabadi, A.R.; Shahabi, H. A comprehensive investigation of the causes of drying and increasing saline dust in the Urmia Lake, northwest Iran, via ground and satellite observations, synoptic analysis and machine learning models. *Ecol. Inform.* **2023**, *78*, 102355. [CrossRef]
47. Salimi, H.; Mirabdolah Lavasani, A.; Ahmadi-Danesh-Ashtiani, H.; Fazaeli, R. Effect of dust concentration, wind speed, and relative humidity on the performance of photovoltaic panels in Tehran. *Energy Sources Part A Recovery Util. Environ. Eff.* **2023**, *45*, 7867–7877.
48. Gholami, A.; Ameri, M.; Zandi, M.; Ghoachani, R.G.; Eslami, S.; Pierfederici, S. Photovoltaic potential assessment and dust impacts on photovoltaic systems in Iran. *IEEE J. Photovolt.* **2020**, *10*, 824–837.
49. Zoljoodi, M.; Didevarasl, A.; Saadatabadi, A.R. Dust events in the western parts of Iran and the relationship with drought expansion over the dust-source areas in Iraq and Syria. *Atmos. Clim. Sci.* **2013**, *3*, 321–336.
50. Cao, H.; Liu, J.; Wang, G.; Yang, G.; Luo, L. Identification of sand and dust storm source areas in Iran. *J. Arid. Land* **2015**, *7*, 567–578.
51. Abdi Vishkaee, F.; Flamant, C.; Cuesta, J.; Oolman, L.; Flamant, P.; Khalesifard, H.R. Dust transport over Iraq and northwest Iran associated with winter Shamal: A case study. *J. Geophys. Res. Atmos.* **2012**, *117*, 1–14.
52. Modarres, R.; Sadeghi, S. Spatial and temporal trends of dust storms across desert regions of Iran. *Nat. Hazards* **2018**, *90*, 101–114. [CrossRef]
53. Rashki, A.; Middleton, N.J.; Goudie, A.S. Dust storms in Iran–Distribution, causes, frequencies and impacts. *Aeolian Res.* **2021**, *48*, 100655.
54. Parno, R.; Meshkatee, A.H.; Mobarak Hassan, E.; Hamzeh, N.H.; Chel Gee Ooi, M.; Habibi, M. Investigating the Role of the Low-Level Jet in Two Winters Severe Dust Rising in Southwest Iran. *Atmosphere* **2024**, *15*, 400. [CrossRef]
55. Gholampour, A.; Nabizadeh, R.; Hassanvand, M.S.; Taghipour, H.; Nazmara, S.; Mahvi, A.H. Characterization of saline dust emission resulted from Urmia Lake drying. *J. Environ. Health Sci. Eng.* **2015**, *13*, 82. [CrossRef] [PubMed]
56. Boroughani, M.; Hashemi, H.; Hosseini, S.H.; Pourhashemi, S.; Berndtsson, R. Desiccating Lake Urmia: A new dust source of regional importance. *IEEE Geosci. Remote Sens. Lett.* **2019**, *17*, 1483–1487. [CrossRef]

57. Abadi, A.R.S.; Hamzeh, N.H.; Shukurov, K.; Opp, C.; Dumka, U.C. Long-term investigation of aerosols in the Urmia Lake region in the Middle East by ground-based and satellite data in 2000–2021. *Remote Sens.* **2022**, *14*, 3827. [CrossRef]
58. Hamzeh, N.H.; Abadi, A.R.S.; Alam, K.; Shukurov, K.A.; Opp, C. Long-Term Wind and Air Temperature Patterns in the Southeastern Region of Iran through Model Simulation and Ground Observations. *Atmosphere* **2024**, *15*, 993. [CrossRef]
59. Effati, M.; Bahrami, H.A.; Gohardoust, M.; Babaeian, E.; Tuller, M. Application of satellite remote sensing for estimation of dust emission probability in the Urmia Lake Basin in Iran. *Soil Sci. Soc. Am. J.* **2019**, *83*, 993–1002. [CrossRef]
60. Ghale, Y.A.G.; Tayanc, M.; Unal, A. Dried bottom of Urmia Lake as a new source of dust in the northwestern Iran: Understanding the impacts on local and regional air quality. *Atmos. Environ.* **2021**, *262*, 118635. [CrossRef]
61. Abadi, A.R.S.; Shukurov, K.A.; Hamzeh, N.H.; Kaskaoutis, D.G.; Opp, C.; Shukurova, L.M.; Ghasabi, Z. Dust events over the Urmia Lake Basin, NW Iran, in 2009–2022 and their potential sources. *Remote Sens.* **2024**, *16*, 2384. [CrossRef]
62. Karimzadeh, S.; Taghizadeh, M.M. Potential of dust emission resources using small wind tunnel and GIS: Case study of Bakhtegan playa, Iran. *Appl. Water Sci.* **2019**, *9*, 174. [CrossRef]
63. Mozafari, M.; Hosseini, Z.; Fijani, E.; Eskandari, R.; Siahpoush, S.; Ghader, F. Effects of climate change and human activity on lake drying in Bakhtegan Basin, southwest Iran. *Sustain. Water Resour. Manag.* **2022**, *8*, 109. [CrossRef]
64. Soleimani Sardoo, F.; Hosein Hamzeh, N.; Karami, S.; Nateghi, S.; Hashemi Nezhad, M. Emission and transport of dust particles in Jazmourian basin (Case study: Dust storm 24–26 November 2016). *J. Clim. Res.* **2022**, *1400*, 41–54.
65. Kordavani, M.; Ramesht, M.H.; Jahanyan, S.; Karimi, A. Environmental Reverse Engineering in Simulation of Dynamic Systems Case study: Reconstructing the Ancient Environment of Lake Jazmourian. *Geogr. Dev.* **2025**, *22*, 1–24.
66. Zarasvandi, A.; Carranza, E.J.M.; Moore, F.; Rastmanesh, F. Spatio-temporal occurrences and mineralogical–geochemical characteristics of airborne dusts in Khuzestan Province (southwestern Iran). *J. Geochem. Explor.* **2011**, *111*, 138–151.
67. Daniali, M.; Karimi, N. Spatiotemporal analysis of dust patterns over Mesopotamia and their impact on Khuzestan province, Iran. *Nat. Hazards* **2019**, *97*, 259–281.
68. Banks, J.R.; Brindley, H.E.; Stenchikov, G.; Schepanski, K. Satellite retrievals of dust aerosol over the Red Sea and the Persian Gulf (2005–2015). *Atmos. Chem. Phys.* **2017**, *17*, 3987–4003.
69. Karami, S.; Hamzeh, N.H.; Alam, K.; Noori, F.; Abadi, A.R.S. Spatio-temporal and synoptic changes in dust at the three islands in the Persian Gulf region. *J. Atmos. Sol. Terr. Phys.* **2021**, *214*, 105539.
70. Ghafarian, P.; Kabiri, K.; Delju, A.H.; Fallahi, M. Spatio-temporal variability of dust events in the northern Persian Gulf from 1991 to 2020. *Atmos. Pollut. Res.* **2022**, *13*, 101357. [CrossRef]
71. Rashki, A.; Kaskaoutis, D.G.; Rautenbach, C.D.; Eriksson, P.G.; Qiang, M.; Gupta, P. Dust storms and their horizontal dust loading in the Sistan region, Iran. *Aeolian Res.* **2012**, *5*, 51–62. [CrossRef]
72. Rashki, A.; Kaskaoutis, D.G.; Francois, P.; Kosmopoulos, P.G.; Legrand, M.J.A.R. Dust-storm dynamics over Sistan region, Iran: Seasonality, transport characteristics and affected areas. *Aeolian Res.* **2015**, *16*, 35–48.
73. Kaskaoutis, D.G.; Rashki, A.; Houssos, E.E.; Goto, D.; Nastos, P.T. Extremely high aerosol loading over Arabian Sea during June 2008: The specific role of the atmospheric dynamics and Sistan dust storms. *Atmos. Environ.* **2014**, *94*, 374–384.
74. Rezazadeh, M.; Irannejad, P.; Shao, Y. Climatology of the Middle East dust events. *Aeolian Res.* **2013**, *10*, 103–109. [CrossRef]
75. Nikfal, A.; Ranjbar Saadatabadi, A.; Karami, S.; Sehatkashani, S. Capabilities of the WRF-Chem model in estimating the concentration of dust–A case study of a dust storm in Tehran. *Environ. Sci.* **2017**, *15*, 115–126.
76. Nabavi, S.O.; Haimberger, L.; Samimi, C. Sensitivity of WRF-chem predictions to dust source function specification in West Asia. *Aeolian Res.* **2017**, *24*, 115–131.
77. Dong, Z.; Yuan, M.H.; Su, F.C.; Zhang, J.F.; Sun, J.B.; Zhang, R.Q. Spatiotemporal Variations in Fine Particulate Matter and the Impact of Air Quality Control in Zhengzhou. *Huan Jing Ke Xue Huanjing Kexue* **2021**, *42*, 2179–2189.
78. Rizza, U.; Miglietta, M.M.; Mangia, C.; Ielpo, P.; Morichetti, M.; Iachini, C.; Virgili, S.; Passerini, G. Sensitivity of WRF-Chem model to land surface schemes: Assessment in a severe dust outbreak episode in the Central Mediterranean (Apulia Region). *Atmos. Res.* **2018**, *201*, 168–180. [CrossRef]
79. Song, H.; Wang, K.; Zhang, Y.; Hong, C.; Zhou, S. Simulation and evaluation of dust emissions with WRF-Chem (v3. 7.1) and its relationship to the changing climate over East Asia from 1980 to 2015. *Atmos. Environ.* **2017**, *167*, 511–522. [CrossRef]
80. Teixeira, J.C.; Carvalho, A.C.; Tuccella, P.; Curci, G.; Rocha, A. WRF-chem sensitivity to vertical resolution during a saharan dust event. *Phys. Chem. Earth Parts A/B/C* **2016**, *94*, 188–195.
81. LeGrand, S.L.; Polashenski, C.; Letcher, T.W.; Creighton, G.A.; Peckham, S.E.; Cetola, J.D. The AFWA dust emission scheme for the GOCART aerosol model in WRF-Chem v3.8.1. *Geosci. Model Dev.* **2019**, *12*, 131–166.
82. Yuan, T.; Chen, S.; Huang, J.; Zhang, X.; Luo, Y.; Ma, X.; Zhang, G. Sensitivity of simulating a dust storm over Central Asia to different dust schemes using the WRF-Chem model. *Atmos. Environ.* **2019**, *207*, 16–29.
83. Chen, S.; Yuan, T.; Zhang, X.; Zhang, G.; Feng, T.; Zhao, D.; Zang, Z.; Liao, S.; Ma, X.; Jiang, N.; et al. Dust modeling over East Asia during the summer of 2010 using the WRF-Chem model. *J. Quant. Spectrosc. Radiat. Transf.* **2018**, *213*, 1–12.

84. Wang, D.; Zhang, F.; Yang, S.; Xia, N.; Ariken, M. Exploring the spatial-temporal characteristics of the aerosol optical depth (AOD) in Central Asia based on the moderate resolution imaging spectroradiometer (MODIS). *Environ. Monit. Assess.* **2020**, *192*, 383.
85. Dadashi-Roudbari, A.; Ahmadi, M. Evaluating temporal and spatial variability and trend of aerosol optical depth (550 nm) over Iran using data from MODIS on board the Terra and Aqua satellites. *Arab. J. Geosci.* **2020**, *13*, 277. [CrossRef]
86. Sharma, V.; Ghosh, S.; Singh, S.; Vishwakarma, D.K.; Al-Ansari, N.; Tiwari, R.K.; Kuriqi, A. Spatial variation and relation of aerosol optical depth with LULC and spectral indices. *Atmosphere* **2022**, *13*, 1992. [CrossRef]
87. Chin, M.; Diehl, T.; Ginoux, P.; Malm, W. Intercontinental transport of pollution and dust aerosols: Implications for regional air quality. *Atmos. Chem. Phys.* **2007**, *7*, 5501–5517.
88. Marticorena, B.; Bergametti, G. Modeling the atmospheric dust cycle: 1. Design of a soil-derived dust emission scheme. *J. Geophys. Res.* **1995**, *100*, 16415–16430.
89. Kawamura, R. Study on sand movement by wind. *Rept. Inst. Sci. Technol.* **1951**, *5*, 95–112.
90. Gillette, D.A. Environmental Factors Affecting Dust Emissions by Wind Erosion. In *Saharan Dust*; Morales, C., Ed.; John Wiley: New York, NY, USA, 1979; pp. 71–94.
91. Hamidi, M.; Kavianpour, M.R.; Shao, Y. Numerical simulation of dust events in the Middle East. *Aeolian Res.* **2014**, *13*, 59–70.
92. Fountoukis, C.; Harshvardhan, H.; Gladich, I.; Ackermann, L.; Ayoub, M.A. Anatomy of a severe dust storm in the Middle East: Impacts on aerosol optical properties and radiation budget. *Aerosol Air Qual. Res* **2020**, *20*, 155–165.
93. Middleton, N.J. Dust storms in the Middle East. *J. Arid Environ.* **1986**, *10*, 83–96.
94. Alam, K.; Trautmann, T.; Blaschke, T.; Subhan, F. Changes in aerosol optical properties due to dust storms in the Middle East and Southwest Asia. *Remote Sens. Environ.* **2014**, *143*, 216–227.
95. Klingmüller, K.; Pozzer, A.; Metzger, S.; Stenchikov, G.L.; Lelieveld, J. Aerosol optical depth trend over the Middle East. *Atmos. Chem. Phys.* **2016**, *16*, 5063–5073.
96. Shaheen, A.; Wu, R.; Lelieveld, J.; Yousefi, R.; Aldabash, M. Winter AOD trend changes over the Eastern Mediterranean and Middle East region. *Int. J. Climatol.* **2021**, *41*, 5516–5535.
97. Mohammadpour, K.; Sciortino, M.; Kaskaoutis, D.G. Classification of weather clusters over the Middle East associated with high atmospheric dust-AODs in West Iran. *Atmos. Res.* **2021**, *259*, 105682.
98. Mesbahzadeh, T.; Ahmadi, H. Investigation of sand drift potential (case study: Yazd–Ardakan plain). *J. Agric. Sci. Technol.* **2012**, *14*, 919–928.
99. Behrooz, R.D.; Esmaili-Sari, A.; Bahramifar, N.; Kaskaoutis, D.G. Analysis of the TSP, PM10 concentrations and water-soluble ionic species in airborne samples over Sistan, Iran during the summer dusty period. *Atmos. Pollut. Res.* **2017**, *8*, 403–417.
100. Al-Dousari, A.; Doronzo, D.; Ahmed, M. Types, indications and impact evaluation of sand and dust storms trajectories in the Arabian Gulf. *Sustainability* **2017**, *9*, 1526. [CrossRef]
101. Ahmady-Birgani, H.; McQueen, K.G.; Mirnejad, H. Characteristics of mineral dust impacting the Persian Gulf. *Aeolian Res.* **2018**, *30*, 11–19.
102. Aba, A.; Al-Dousari, A.M.; Ismaeel, A. Atmospheric deposition fluxes of 137Cs associated with dust fallout in the northeastern Arabian Gulf. *J. Environ. Radioact.* **2018**, *192*, 565–572.
103. Zhao, J.; Ma, X.; Wu, S.; Sha, T. Dust emission and transport in Northwest China: WRF-Chem simulation and comparisons with multi-sensor observations. *Atmos. Res.* **2020**, *241*, 104978.
104. Tsarpalis, K.; Papadopoulos, A.; Mihalopoulos, N.; Spyrou, C.; Michaelides, S.; Katsafados, P. The implementation of a mineral dust wet deposition scheme in the GOCART-AFWA module of the WRF model. *Remote Sens.* **2018**, *10*, 1595. [CrossRef]
105. Karami, S.; Hamzeh, N.H.; Kaskaoutis, D.G.; Rashki, A.; Alam, K.; Ranjbar, A. Numerical simulations of dust storms originated from dried lakes in central and southwest Asia: The case of Aral Sea and Sistan Basin. *Aeolian Res.* **2021**, *50*, 100679.